

**Research Paper**

**Correspondence to:**  
Laoura Athanasiadou  
[karkjul83@gmail.com](mailto:karkjul83@gmail.com)

**DOI number:**  
<http://dx.doi.org/10.12681/bgsg.20948>

**Keywords:**  
karst, fresh water outflows,  
thermal image Landsat 8,  
Evia

**Citation:**  
Athanasiadou L., Psomiadis  
E. and Stamatis G. (2020),  
Thermal Remote Sensing for  
Water Outflows Detection  
and Determination of the  
Role of Lineaments in  
Underground Hydrodynamics  
of Evia Island, Central  
Greece. Bulletin Geological  
Society of Greece, 56, 100-  
132.

**Publication History:**  
Received: 31/07/2019  
Accepted: 07/04/2020  
Accepted article online:  
16/04/2020

The Editor wishes to thank  
two anonymous reviewers  
for their work with the  
scientific reviewing of the  
manuscript and Ms  
Emmanouela  
Konstantakopoulou for  
editorial assistance.

©2020. The Authors  
This is an open access  
article under the terms of  
the Creative Commons  
Attribution License, which  
permits use, distribution  
and reproduction in any  
medium, provided the  
original work is properly  
cited

**THERMAL REMOTE SENSING FOR WATER OUTFLOWS  
DETECTION AND DETERMINATION OF THE ROLE OF  
LINEAMENTS IN UNDERGROUND HYDRODYNAMICS OF EVIA  
ISLAND, CENTRAL GREECE**

**Laoura Athanasiadou<sup>1</sup>, Emmanouil Psomiadis<sup>1</sup>, Georgios Stamatis<sup>1</sup>.**

<sup>1</sup>Laboratory of Mineralogy & Geology, Department of Natural Resources Management  
& Agricultural Engineering, Agricultural University of Athens, Iera Odos 75, Athens,  
Greece, [karkjul83@gmail.com](mailto:karkjul83@gmail.com), [mpsomiadis@gmail.com](mailto:mpsomiadis@gmail.com), [stamatis@aua.gr](mailto:stamatis@aua.gr).

**Abstract**

*The coastal karst system of Evia Island is developed due to the extended presence of carbonate formations, discharges into the sea either at the coastal zone or via submarine springs, having a direct relation to the tectonic system of the area. Thermal infrared remote sensing has been proved its capability in monitoring thermal differentiations of coastal water plumes. This work aims to locate the freshwater outflows through remote sensing and specific with the use of Landsat's 8 thermal images and to reveal how the lineaments of the area control this karstification process. L8 contains two thermal bands (Band 10, high gain and Band 11, low gain) with resolution 30m which record the scattering of infrared radiation from the sea surface. Spectral Band 10 was selected due to the high gain characteristics which provide more suitable radiometric resolution (sensitivity). Finally, combining thermal images with geological maps, sea surface temperature (SST) maps have been created.*

**Keywords:** karst, fresh water outflows, thermal image Landsat 8, Evia

**Περίληψη**

*Ένα τμήμα των ακτών της νήσου Ευβοίας καλύπτεται από ανθρακικά πετρώματα. Στους σχηματισμούς αυτούς, αναπτύσσονται υδροφόρα καρστικά συστήματα. Η καρστικοποίηση τους είναι συνέπεια του συνδυασμού των τελευταίων τεκτονικών κινήσεων της Αλπικής ορογένεσης και των κατακόρυφων ευστατικών κινήσεων του Τεταρτογενούς, με αποτέλεσμα την εμφάνιση παράκτιων και υφάλμυρων καρστικών*

πηγών σε πολλές περιοχές της Εύβοιας. Το επιφανειακό νερό εισέρχεται στους βαθύτερους ορίζοντες και εμφανίζεται στη θάλασσα με τη μορφή παράκτιων ή υποθαλάσσιων πηγών. Η Θερμική Τηλεπισκόπηση έχει αποδείξει την ικανότητα της να παρακολουθεί τις θερμικές διαφοροποιήσεις των υδατοκηλίδων (*water plumes*). Σκοπός της εργασίας, είναι ο εντοπισμός των παράκτιων και υποθαλάσσιων πηγών, χρησιμοποιώντας θερμικές εικόνες από τον δορυφόρο Landsat 8, και η διερεύνηση της σύνδεσης της καρστικοποίηση με τις διακλάσεις που εμφανίζονται στην περιοχή και κατ' επέκταση με το πως αυτές επηρεάζουν την διακίνηση του υπόγειου νερού. Ο δορυφόρος περιλαμβάνει δύο θερμικά (φασματικά κανάλια 10 και 11 με χωρική ανάλυση 30 m) τα οποία καταγράφουν την σκεδαζόμενη ακτινοβολία από την υδάτινη επιφάνεια. Στην παρούσα εργασία χρησιμοποιήθηκε το φασματικό κανάλι 10 (10.60  $\mu\text{m}$  – 11.19  $\mu\text{m}$ ) το οποίο λόγω της υψηλής απολαβής λήψης παρέχει καλύτερα αποτελέσματα στην θερμική αποτύπωση των διαφυγών. Ο συνδυασμός των θερμικών εικόνων και των γεωλογικών χαρτών είχε σαν αποτέλεσμα τη δημιουργία θεματικών χαρτών που απεικονίζουν τα σημεία ενδιαφέροντος.

*Λέξεις κλειδιά:* καρστ, εκφορτίσεις γλυκού νερού, θερμικές εικόνες Landsat 8, Εύβοια

## 1. INTRODUCTION

The growing human (urban and rural) demands on freshwater in semi-arid regions, implies that the exploration of new locations of possible groundwater discharge and accumulation are critical for augmenting the limited water resources (Migiros et al., 2008). The geographical location of Greece, with its general geomorphological composition, and its climate and hydrological conditions, characterises it as an almost anhydrous country, which is often substantiated by the dry-warm climatic environment of most of the country (UNESCO, 1978). In Greece, 30% of the land surface is covered by carbonate formations (Kallioras et al., 2016), having a numerous of water-rich karst resources that probably could solve the water supply and irrigation problem in coastal and island regions, even though most of them cannot be utilised due to their salinity. Brackish waters should be considered as available water resources, since desalination is regarded as one of humanity's earliest forms of water treatment, providing excessive solution throughout the world today. Nearly 70% of the world's population lives in coastal areas, and most of these people depend on coastal aquifers for freshwater (Stefouli and Tsombos, 2004). Submarine groundwater discharge (SGD) along coasts is a worldwide phenomenon that occurs where hydraulic gradients and permeability (hydraulic characteristics) are sufficiently large to cause lateral and upward flow of

groundwater, primarily because of differences in density of groundwater with low salinity and seawater (Fleury et al., 2007; Meijerink et al., 2007).

To detect and map this substantial groundwater outflows several advanced space-borne sensors with different spatial, spectral, temporal and thermal resolutions have been utilised aimed at monitoring the thermal aspect of coastal waters (Parcharidis et al., 1998; Migiros et al., 2008). The usage of modern technologies, such as remote sensing and geographic information systems (GIS), has expanded the potential of temperature maps and fresh water outflows monitoring (Theilen-Willige et al., 2014). Thermal remote sensing based on recording the electromagnetic radiation in the thermal infrared region (TIR) emitted by surface objects as a function of their temperature in two spectral windows: 3  $\mu\text{m}$  -4  $\mu\text{m}$  and 10.5  $\mu\text{m}$  - 12.5  $\mu\text{m}$  (Meijerink et al., 2007). The thermal data of Landsat satellites provide information on surface temperature differentiation and can be used to detect and delineate freshwater discharges, and such contribute to hydrologic and geothermal studies (Ganas et al., 2003; Ganas & Lagios, 2003). The outflow of colder groundwater into warmer seawater results in plumes at sea surface in the zones of groundwater discharge (Tcherepanov et al., 2005). Thus, the colder the object, the lower the amount of electromagnetic radiation. Thermal Infrared images are used to evaluate large areas in a short time and acquire useful information and measurements of the Earth's land and sea surface temperatures (Stefouli et al. 2013).

The Earth observation satellite that used in this study is LANDSAT 8 (L8). Data collected by the satellite system, are available to download free of charge from the United States Geological Survey website (USGS - <https://earthexplorer.usgs.gov/>). The thermal Infrared Sensor (TIRS) of L8 is ideal, having high spatial (30 m) and thermal ( $< 0.4^\circ \text{C}$ ) resolution for monitoring thermal plumes. TIRS has two thermal bands (10 and 11) in the range of 10.0–13.0  $\mu\text{m}$  and according to the recommendations of USGS, only Band 10 was utilized, due to band 11 more significant calibration uncertainties. The goal of this work is to evaluate the capability of the remote sensing data and methods to detect the groundwater outflows in Evia island and to correlate these discharges with the geologic conditions and the role of the tectonics in the alimentation of the aquifer system of the study area (Ganas et al., 2005; Lancia et al., 2018; Kuz'mina and Novopashina, 2018).

### **1.1 Sea Surface Temperature (SST)**

The sea surface temperature (SST) is one of the important oceanic environmental factors in determining the change of marine environments and ecological activities

(Kang et al, 2014). More specifically is a significant parameter for biological, chemical and physical processes occurring within water. The SST represents gradient in the first several centimeters of the water, which is usually sustained by the atmospheric heat flux (Donlon et al., 2002). There are various methods of estimating SST such as shipboard measurements, thermometers in drifting buoys and from thermal bands. First two, are time-consuming and expensive but the results are accurate. Thermal images from satellite or aircraft platforms provide a regular sampling of SST, improving measurement capability (Tang et al., 2003) but the radiation emanates from the top “skin” of the ocean approximately the top 0.01 mm or less, which may not represent the bulk temperature of the upper metre of sea due primarily to effects of solar surface heating during the daytime, reflected radiation, as well as sensible heat loss and surface evaporation. Also, it cannot be used if there are clouds in the area.

SST measurements from thermal bands have been used to detect a) ground water discharge areas, based on the thermal anomalies that appear on sea surface (Parcharidis et al., 1998; Karfakis et al., 1998; Karfakis and Nikolakopoulos, 2003; Tcherepanov et al., 2005; Lamaro et al., 2013; Mallast et al., 2013; Stefanakis et al., 2018), b) potential fishing zone (PFZ). Water temperature is an important factor in determining species distribution. SST maps can be used to identify cold water upwelling of nutrient-rich water and to locate boundary areas between warm and cold waters where certain species are known to congregate (Das et al, 2010), c) oil spills. Oil of thicknesses greater than about 10  $\mu\text{m}$ , absorbs light in the visible region and re-radiates a portion of this in the infrared spectrum, mostly in the 8–14  $\mu\text{m}$  wavelengths. Solar-heated oil will emit infrared radiation as oil shows greater infrared emissivity than water. Thick oil appears heated or “hot” compared to the surrounding water in infrared images, intermediate thickness layers of oil appear “cool”, and thinner layers of oil or sheens are not distinguished (Fingas and Brown, 2018), d) eutrophication. The interannual variability of sea surface temperature (SST) is found to be a good indicator of phytoplankton abundance (Gittings et al., 2018), e) weather phenomena. Sea surface temperature affects the behavior of the Earth's atmosphere above and is important in determining the formation of sea fog and sea breezes, for tropical cyclogenesis (El Niño), etc.

## 1.2 Landsat 8 satellite

Landsat 8 is an American Earth observation satellite launched on February 11, 2013, from Vandenberg Air Force Base, California, on an Atlas-V 401 rocket. Originally, called the Landsat Data Continuity Mission (LDCM). It is a collaboration between NASA and the United States Geological Survey (USGS) consisting of *the spacecraft*

and the *ground system*. The spacecraft accommodates two government-furnished instruments forming the Landsat 8 Observatory, OLI and TIRS (<https://landsat.gsfc.nasa.gov/landsat-8/>). The Operational Land Imager (OLI) is a push-broom sensor with a four-mirror telescope and 12-bit quantization, measures in the visible, near infrared, and short-wave infrared portions of the spectrum, with 7 bands. Its images have 15-m panchromatic and 30-m multi-spectral spatial resolutions along a 185 km wide swath, covering wide areas of the Earth's landscape while providing sufficient resolution to distinguish features like urban centers, farms, forests and other land uses. The entire Earth will fall within view once every 16 days due to Landsat 8's near-polar orbit. The Thermal Infrared Sensor (TIRS) measures surface temperature in two thermal bands with a new technology that applies quantum physics to detect heat, which use Quantum Well Infrared Photodetectors (QWIPs) to detect long wavelengths of light emitted by the Earth whose intensity depends on surface temperature. Like OLI, TIRS employs a push broom sensor design with a 185-kilometre swath width. TIRS bands 10-11 data are collected at 100 m but resampled to 30 m to match OLI multispectral bands. Also have a 16 - day repeat cycle. The Ground System includes all of the ground-based assets needed to operate the Landsat 8 observatory. The primary components are the Mission Operations Element, Collection Activity Planning Element, Ground Network Element, and the Data Processing and Archive System.

### 1.3 Tectonics and groundwater system

The evolution of karst surface landforms and subsurface drainage systems in the aquifers have been conditioned in geological time by tectonics. The Alpine tectonic phases with alternating compression and extension contributed to the development of different karst - genetic levels. Tectonic strains opened and possibly closed some fractures, allowing (or preventing) water to flow through parts of the karst massive (Hauselmann, 1999). Furthermore, determinates the degree of carbonate disintegration that contributes to the groundwater circulation. In inactive tectonic areas, the base karst level of the groundwater flow changes over time mainly by the filling up of morphological depressions by recent clastic deposits and also by changes in sea level (Cavinato and De Celles 1999; Petitta 2009). In most aquifers, water circulates and accumulates in the original voids of the rock: the pores or discontinuities produced by the deformations. In conclusion, geological history has proven to us that the change of sea level or/and movements imposed by plate tectonics modify external conditions by increasing or decreasing the ability of underground flows to create a network of conduits and discharge freshwater via coastal or submarine springs.

## 2. STUDY AREA

### 2.1 Physical Geography

The study area includes the island of Evia, where, together with Skyros, a part of the Boeotian coast and the surrounding islands constitute the Regional Unit of Evia (Fig. 1). The area of the island is 3654 km<sup>2</sup> and the coastline length is 678 km. Evia is the second largest island in Greece and the sixth largest in the Mediterranean. It extends along the Southeastern mainland of Sterea Hellas (Central Greece), from the Maliakos Gulf to the coast of Rafina (Attika), separated by the Evian Gulf (Fig. 1).

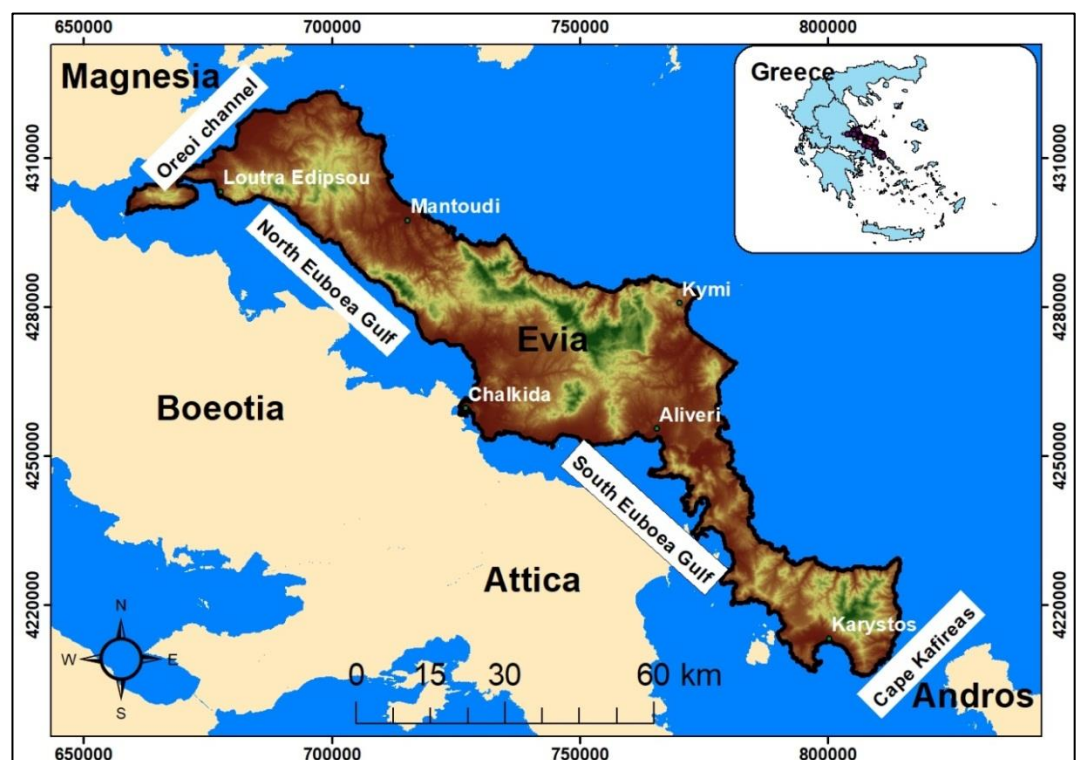


**Fig. 1:** Study area, Evia Island (Central Greece).

### 2.2 Geological Setting

Evia consists of the following units (Katsikatsos, 1992; Fig. 2):

- 1) Post Alpine formations

The sequence is overlain by Lower Miocene to Upper Pliocene Neogene and Alluvial deposits (which outcrop on the adjacent to marine deposits, land areas).

- 2) Unit of Central and Northern Euboea and Skyros

Includes at the lower series a Permian–Triassic volcanoclastic complex with low-grade metamorphic rocks and rift volcanics. This is overlaid by Upper Triassic to Upper

Jurassic limestones (the “Sub-Pelagonian” unit) and finally an ophiolitic nappe is tectonically imposed over the limestones, which was emplaced in the Late Jurassic to Early Cretaceous, and Paleocene to Early Eocene flysch. These Mesozoic formations were also folded during the main phase of the Alpine orogeny (Kelepertsis et al., 2009).

### 3) Unit of Almyropotamos

Belong to the Basal unit. Consisting of Mesozoic to Meso-Eocene coarse-grained marbles of great thickness, passing upwards into metaflysch and schists intercalate in the entire thickness of these marbles.

### 4) Unit of Southern Euboea

It is the tectonic unit under the Pelagonian zone, is metamorphosed and overthrust on the flysch of unit of Almyropotamos. Comprise *the Ochi unit*, which contains glaucophane schist, large bodies of amphibolite and manganese microquartzite, *the Tsakaioi unit*, consisting of schist and amphibolite including large bodies of serpentine and *the Styra unit*, composed of thin plate marble, sipoline, quartzite and amphibolitic schist. Moreover, ophiolitic rocks expand at the base of the Styra – blueschist nappe on top of the Mesozoic – Eocene unit of Almyropotamos (Papanikolaou, 2009).

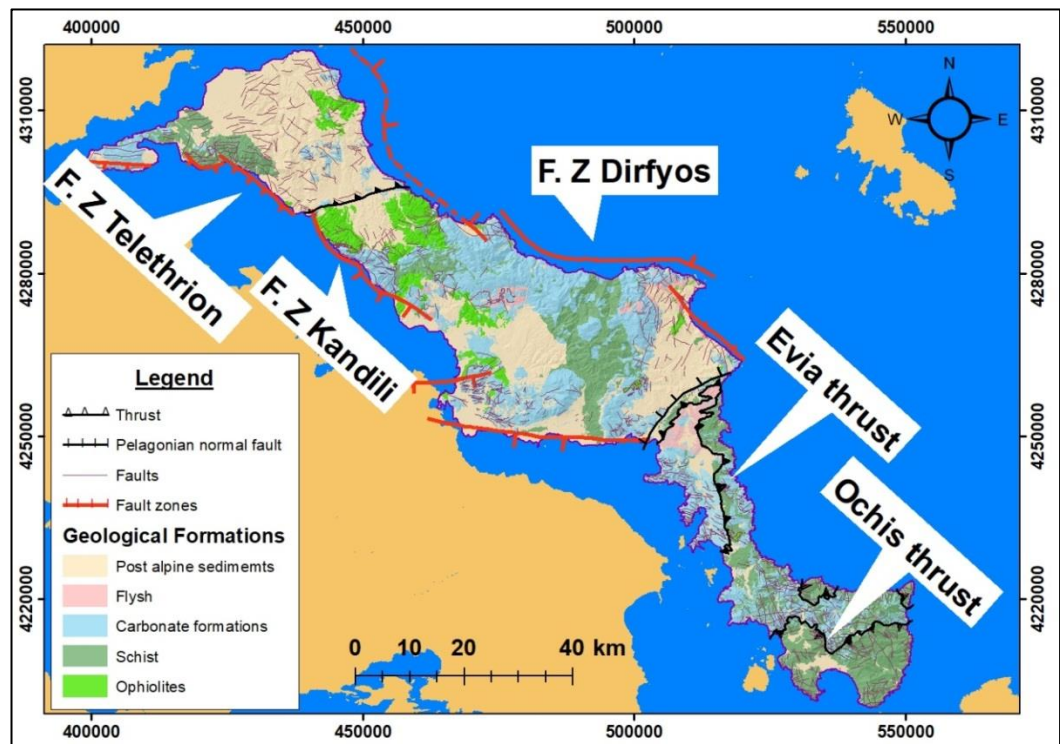


**Fig. 2:** Simplified geological and tectonic map of the study area (based on I.G.M.E maps; Soulios, 1986; Roberts and Jackson, 1991; Lekkas, 2002; Palyvos et al., 2006).

## 2.3 Tectonic Activity

The tectonic evolution of Evia, as well as the wider area, determined the general geomorphological picture of the area and in combination with the stratigraphic column of the formations, played a key role in the movement of groundwater and the appearance of many karst springs. The North Euboea Gulf is considered one of the most active neotectonic structures in Greece (Goldsworthy et al., 2002). The faults structures of the north area correspond to two submarine oppositional zones of normal faults that have an NW-SE orientation and border the mountainous basin of the northern part of the island and divide it from the North Euboea Gulf to the west and the Aegean to the east. The fault zone of Telethron – Kandili is located to the west and inclined to the southwest while the fault zone of Dirfyos is located to north - east and inclined to the east. The submarine faults zones along the east and west coasts are responsible for the geomorphological evolution of the north Evia (Valkanou et al., 2015). Major fault systems with EW, NW, SE and NE – SW orientation are observed in the Central Evia Gulf region. In the wider area of Chalkida, there are faults with E-W and WNW - ESE orientation (Lekkas, 2002). The creation of the South Euboea Gulf is due to the strong tectonic movements, combined with the vertical displacements that have taken place since the Miocene until the present (Korozis, 2011).

## 3. MATERIALS AND METHODOLOGY

### 3.1 Data Collection

The set of data used in the present investigation incorporates images from space-borne observation systems and vector data, includes:

- 18 topographic maps at 1:50.000 scale of the Hellenic Military Geographical Service
- 12 geologic maps at 1:50.000 of Institute of Geology and Mineral Exploration and 40 satellite images of Landsat 8 have been used, mostly cloud - free with a flyover time between 09:04 and 09:06 GMT. In this paper for the specific area, we utilized 12 images – one for every month-with the following characteristics (Table 1).

The images were downloaded free of charge from the site of the United States Geological Survey - *Earth Explorer*. From the data sets, we choose Landsat collection 1- level 1, Landsat 8 OLI/TIRS C1 – Level 1. Digital image processing of the satellite data was carried out using ENVI software (v.5.3 - Harris Geospatial Solutions, USA),

while the manipulation of the spatial information and the digitizing of thematic maps was made using ArcGIS software (v.10.2.1, Environmental Systems Research Institute, Redlands, CA, USA).

**Table 1.** Landsat 8 images features.

| Path/Row   | Grid cell size<br>(Processing level 1) | Datum  | Acquisition Date | Cloud_Cover<br>(%) |
|------------|--|--------|------------------|--------------------|
| 183/033    | 30                                     | WGS 84 | 30/4/2013        | 0.13               |
|            |  |        | 23/10/2013       | 0.55               |
|            |  |        | 8/11/2014        | 0.05               |
|            |  |        | 23/6/2015        | 14.86              |
|            |  |        | 9/7/2015         | 5.05               |
|            |  |        | 28/8/2015        | 1.92               |
|            |  |        | 2/2/2016         | 0.41               |
|            |  |        | 21/3/2016        | 3.65               |
|            |  |        | 29/9/2016        | 1.77               |
|            |  |        | 6/1/2017         | 0.53               |
|            |  |        | 14/5/2018        | 2.19               |
| 24/12/2018 | 2.62                                   |        |                  |                    |

### 3.2 Methods and Analysis

For the detection of groundwater discharge zones in coastal areas, Landsat thermal infrared imagery was used. The study is based on the fact that there is a contrast between ground and surface water. Thermal images were processed using ENVI 5.3 program for conversion DN to temperature (Celsius degrees). More specifically, first processing step included the radiometric correction, converting the digital numbers (DN) to Top of Atmosphere (TOA) Radiance, following the method presented by Chander et al. (2009):

$$L_{\lambda} = M_L * Q_{cat} + A_L \quad (1)$$

Where:

- $L_{\lambda}$  = Spectral radiance (W/ (m<sup>2</sup> \* srad \*  $\mu$ m)): (Watt/(per square metre \*per steradian\*per micrometre)),
- $M_L$  = Radiance multiplicative scaling factor for the band (RADIANCE\_MULT\_BAND\_n from the metadata),
- $A_L$  = Radiance additive scaling factor for the band (RADIANCE\_ADD\_BAND\_n from the metadata) and
- $Q_{cat}$  = Quantized and calibrated standard product pixel values (DN).

The second step was to apply atmospheric correction, which involves the removal of atmospheric effects that contribute to the signal received by the sensors (up to 90% for

water) and these effects change surface water temperature values of  $\pm 2^{\circ}\text{C}$  (Kay et al., 2005). The equation to obtain the surface reflectivity is based on (Chavez., 1988):

$$\rho_{SUP} = \frac{d^2\pi(L_{TOA}-L_o)}{(E_{TOA}\cos\theta_i)} \quad (2)$$

Where:

- $\rho_{SUP}$  = the corrected surface radiance (Watts/ (m<sup>2</sup> \* srad \*  $\mu\text{m}$ )),
- $d$  = the Earth-Sun distance,
- $L_{TOA} = L_{\lambda}$  = the spectral radiance at satellite's sensor,
- $L_o$  = the upwelling atmospheric spectral radiance scattered (based on the minimum values of the histogram for the separate spectral bands),
- $E_{TOA}$  = the solar spectral irradiance on a surface perpendicular to the Sun's rays outside the atmosphere and
- $\theta_i$  = the solar zenith angle.

Afterwards, these values were converted to at – satellite brightness temperature by the inversion of Planck's equation:

$$T = \frac{K_2}{\ln\left(\frac{K_1}{L_{\lambda}} + 1\right)} \quad (3)$$

Where:

- $T$  = Top of atmosphere brightness temperature (Kelvin),
- $L_{\lambda}$  = TOA spectral radiance =  $\rho_{SUP}$  (equation 2), (Watts/ (m<sup>2</sup> \* srad \*  $\mu\text{m}$ )),
- $K_1$  = Band-specific thermal conversion constant from the metadata ( $K_1\_CONSTANT\_BAND\_x$ , where x is the thermal band number), (for Landsat band 10  $K_1 = 774.8853$ ) and
- $K_2$  = Band-specific thermal conversion constant from the metadata ( $K_2\_CONSTANT\_BAND\_x$ , where x is the thermal band number), (for Landsat band 10  $K_2 = 1321.0789$ ).

To estimate SST, the sea surface emissivity must be known, since is a proportionality factor that scales blackbody radiance (Planck's law) to predict emitted radiance and it is the efficiency of transmitting thermal energy across the sea surface into the atmosphere (Manoz et al., 2006). Total radiation from the sea surface into the bottom of the atmosphere is the sum of the surface radiation and the reflection of the atmosphere radiation of the surface. Therefore, it is important to separate the surface

emission from the surface reflection (Konda et al., 1994). Several studies attempted to estimate sea surface emissivity through different methods (Buether and Kern, 1965; Saunders, 1967b, 1968; Mikhaylon and Zolotarev, 1970; Davies et al., 1971; Masuda et al., 1988; Konda et al., 1993). In this paper, we used a value of 0.9885 for water emissivity as calculated by Snyder et al. (1998, 2005). They first proposed a classification – based method by elaborately developing an emissivity knowledge database (10 – 12,3  $\mu\text{m}$ ), used thermal infrared images and radiance was measured by satellite sensor which includes both temperature and emissivity. In the end, they separated emissivity from temperature.

The next to last step of retrieving the SST, is computed as follow (Alshaikh, 2016):

$$T_s = \frac{BT}{\{1 + \left[\left(\frac{\lambda BT}{\rho}\right) \ln \epsilon_\lambda\right]\}} \quad (4)$$

Where:

- $T_s$  = SST in Kelvin,
- BT = Brightness Temperature = T (equation 3) (Kelvin),
- $\lambda$  = the wavelength of emitted radiance (for Landsat 8 is 10.8  $\mu\text{m}$ ),
- $\epsilon_\lambda$  = sea surface emissivity = 0.9885 and
- $\rho = h * (c/\sigma) = 1.438 * 10^{-2} \text{ m} * \text{K}$ , where:  $\sigma$  is the Boltzmann constant ( $1.38 \times 10^{-23} \text{ J/K}$ ),  $h$  is Planck's constant ( $6.626 \times 10^{-34} \text{ J s}$ ) and  $c$  is the velocity of light ( $2.998 \times 10^8 \text{ m/s}$ ).

In the end, values were converted from Kelvin to Celsius, using the equation:

$$\text{Celsius} = \text{Kelvin} - 273.15 \quad (5)$$

Then, the new images (Fig. 3) were imported and manipulated into ArcMap 10.2.1. Before data analysis, initial processing on the raw data is usually carried out to correct for any distortion due to the characteristics of the imaging system and imaging conditions:

- *Radiometric correction* is done to calibrate the pixel values and correct for errors in the values which concludes conversion DN to radiance and converting to At-Satellite Brightness Temperature,
- *Atmospheric correction* for remove the effects of the atmosphere to produce surface reflectance values.

These steps are analyzed above.

- *Geometric correction* is undertaken to avoid geometric distortions from a distorted image and is achieved by establishing the relationship between the image coordinate system and the geographic coordinate system using calibration data of the sensor, measured data of position and attitude, ground control points, atmospheric condition, etc. Also includes the resampling technique of manipulating a digital image and transforming it into another form. We used bilinear interpolation which produces a smoother interpolation than the other methods – based on the four neighboring pixels.

Then, a supervised classification was implemented at the desired temperature ranges, for better detection of thermal anomalies on sea surface (Hemalatha & Varadarajan, 2018). Meant for digital number classification a thorough density slicing procedure was followed to enhance the information gathered from an individual brightness band. The methodology was fulfilled by dividing the range of brightness's in a single band into intervals assigning then each interval to a color. Thus, grayscale values (0-255) are converted into a series of intervals, or slices, and different colors are assigned to each slice.

Moreover, topographic and geological maps were edited to ArcMap. First, a geometric correction was made utilizing ground control points in Hellenic Geodetic Reference System 1987. The resulting maps were employed to extract cartographic information in vector format using the digitization process: cities, geological formations, faults, coastline, contours (digital elevation model was created), etc. Finally, thermal images were combined with geological and topographic maps and sea surface temperature (SST) maps had been created.

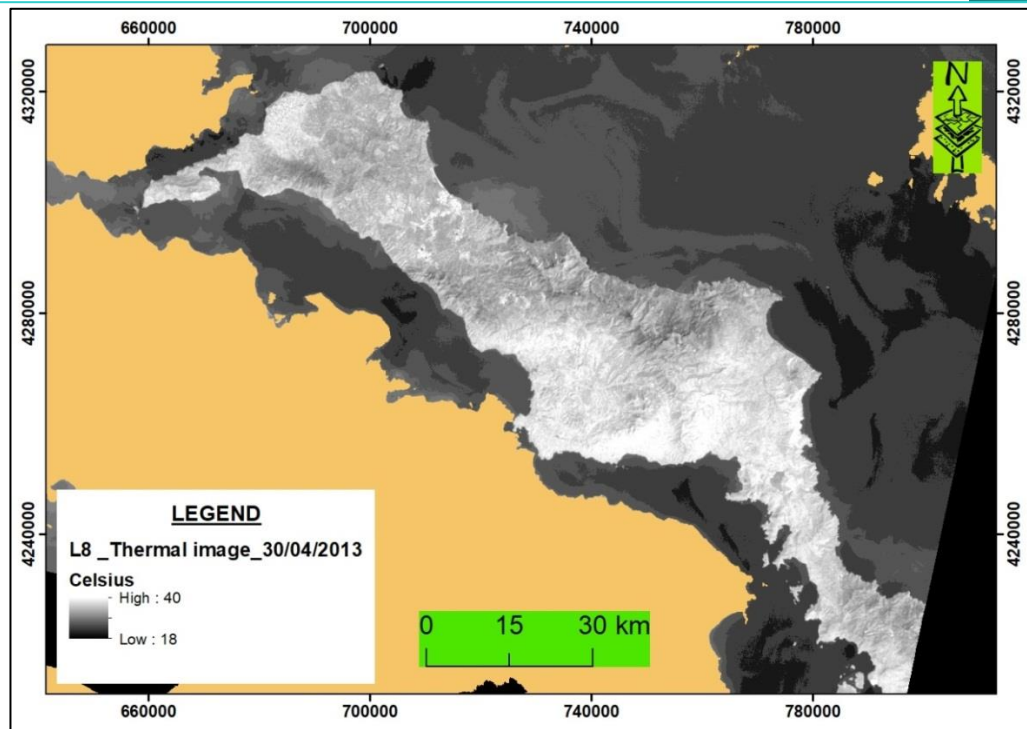


**Fig. 3:** Processed thermal image (band 10 – high gain) of Landsat 8.

#### 4. DISCUSSION

The coastal karst communicates hydraulically with the large carbonaceous masses of the Evia's internal part and is, therefore, being fed additionally. Limestones are characterised by secondary porosity, which allows the circulation of surface water to deeper horizons. It is then discharged into the sea through coastal and submarine springs that appear in tectonic discontinuities. The freshwater outflows are more diluted and cooler concerning seawater, and spread upwards to the sea-surface, creating characteristic water plumes (Astaras, 2001). At thermal images, the darkest tones correlate with the lowest temperatures which are related to the fresh cold-water outflows. In many coastal areas of Evia Island (Metoxi, Xalkida, Marmari, Limni, Vlaxia, Vathiremna, Aliveri), the phenomenon was detected (Fig. 4). In this paper, the Limnionas- Xalatzas area was selected because the spots of discharges are “clearer” than the other areas. Twelve images - one for every month - were chosen from 2013 to 2018, with no cloud cover in the specific area, to see if the phenomenon was prominent through the years (Fig. 5), (Ganas & Stefouli, 1995; Stefouli & Tsombos, 2004; Ompetsanof et al., 2004).

Despite a dry summer that depletes the potential of the karstic aquifers, September rains begin and fill the underground reservoir where are discharged coastal, forming a freshwater “strip” (September, October, November, December and January images), lower in temperature from the sea, along the coast. In January, also two spots of outflows that look like plumes (1 and 2) appear. In February the stripe begins to replace by freshwater “marks” (3, 4 and 5). Afterwards, groundwater receives greater amounts of rain and snow where outflows continue to occur in March, April and May images. Also, hot masses were noticed (yellow arrow). That is because a) the tectonics of area. Seawater penetrates into the fault zone, enters deep depths, where it is heated and through the pressures it rises to the surface of the sea in the form of hot water, and (b) volcanic activity that took place in the Upper Miocene (13 – 17 million years ago). Then begins the dry season where precipitations decrease significantly. However, from June to August images, there are freshwater outflows (13 to 18). This means that the underground system is always full of water and there is a constant flow of groundwater to the sea. It is good to note, that several August images were found that had no outflow spots. This may be because the underground reservoir has stored water but not much to move through the karstic aquifers to the sea. The discharges come from the Underground Water System of karstic aquifer developed in the masses of carbonate rocks of Mount Dirfys in Central Evia and they are related to the fault system of the tectonic discontinuities that prevail in the main tectonic blocks.

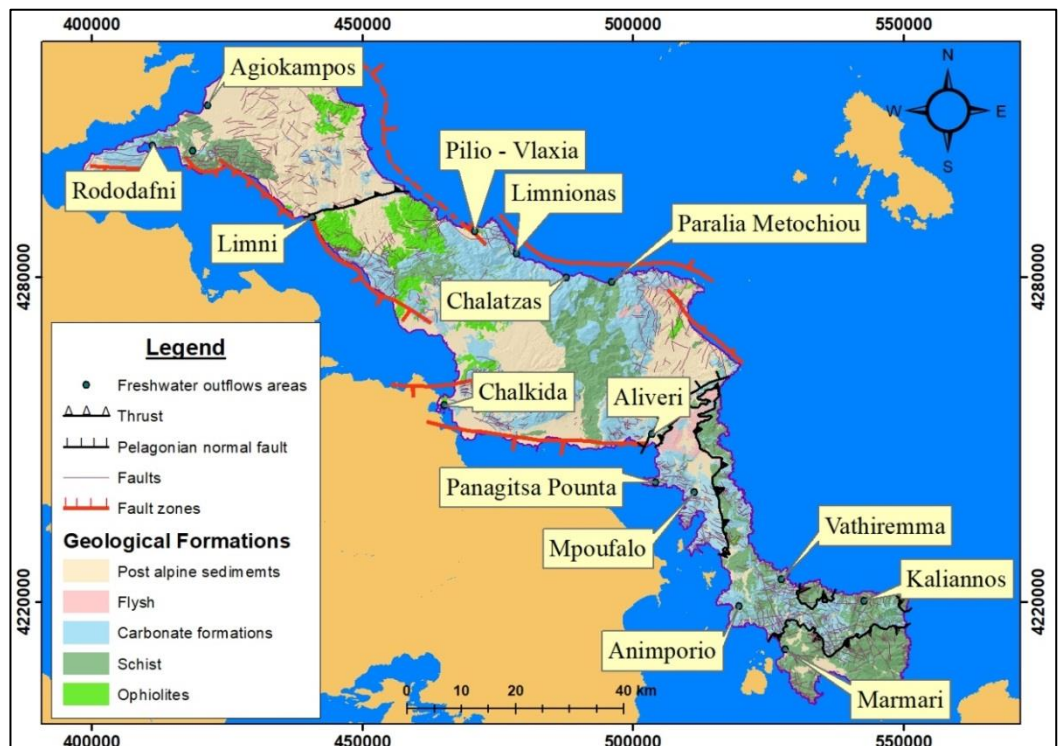
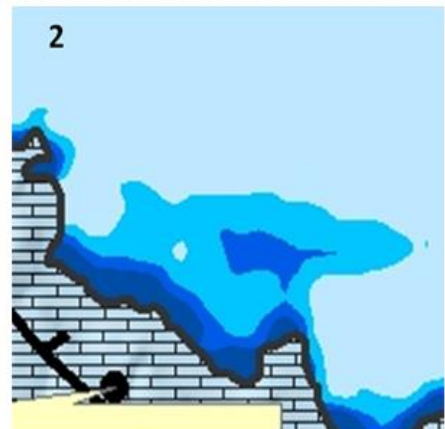
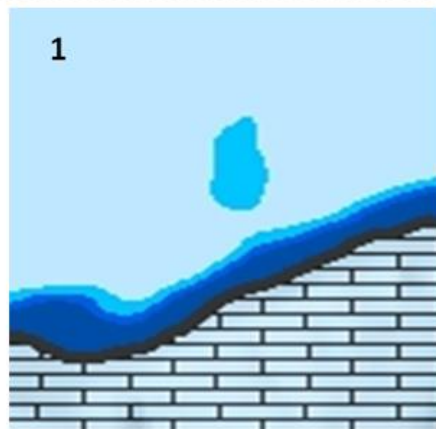
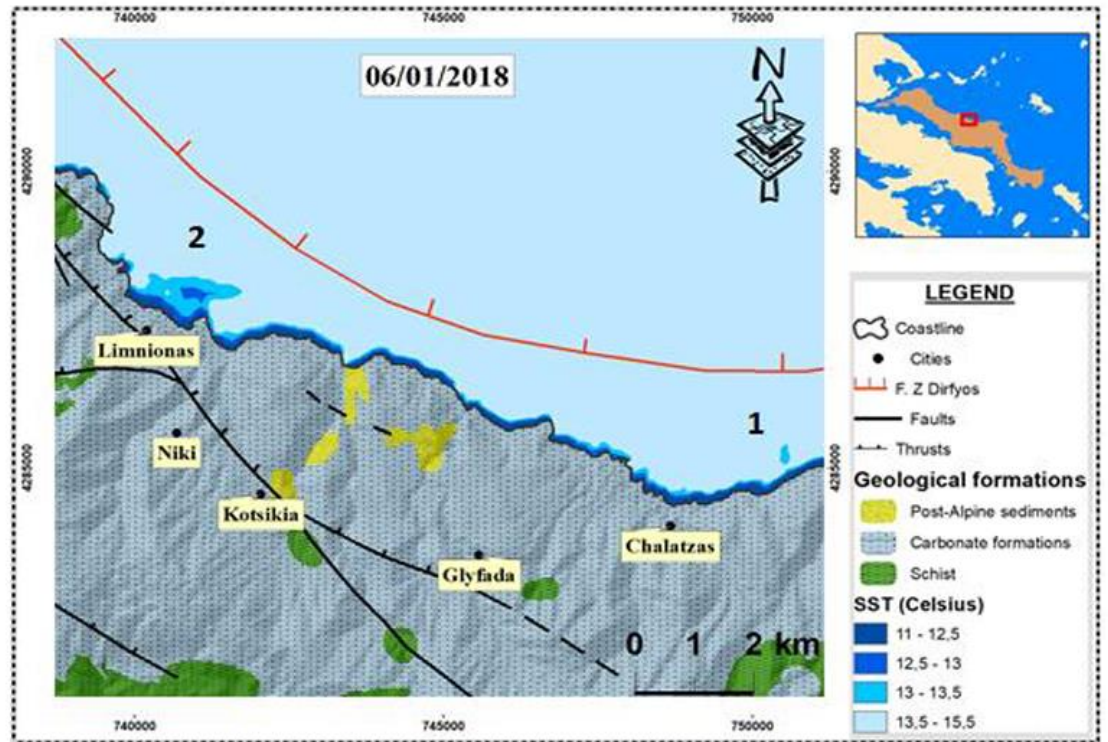
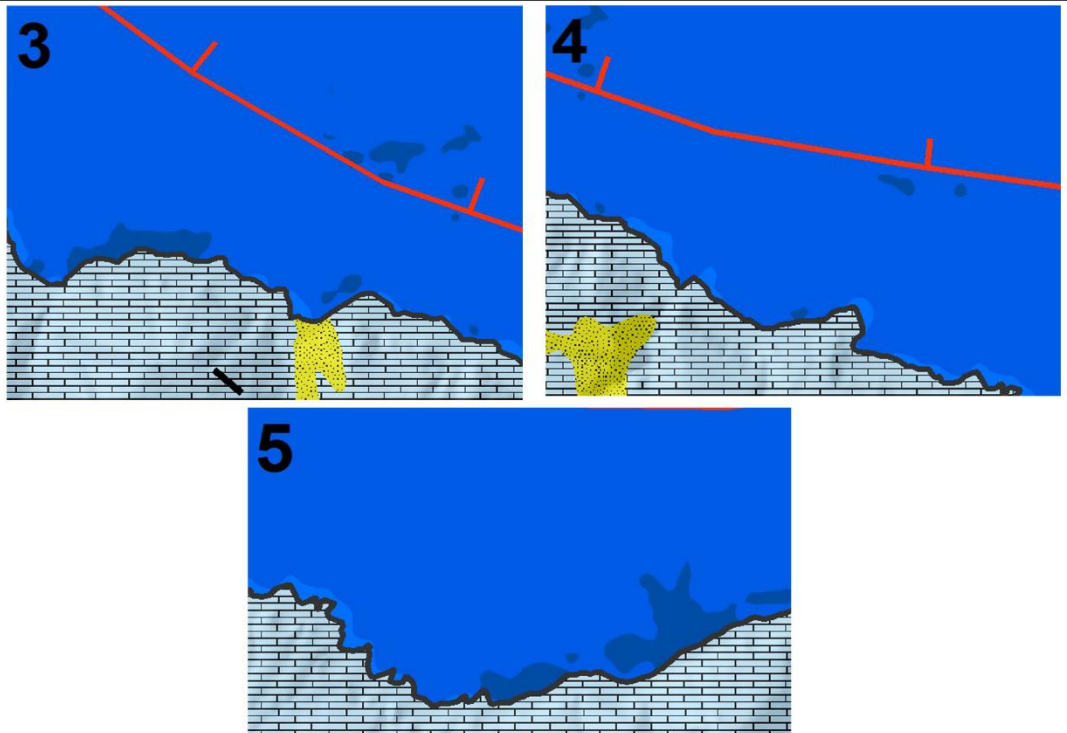
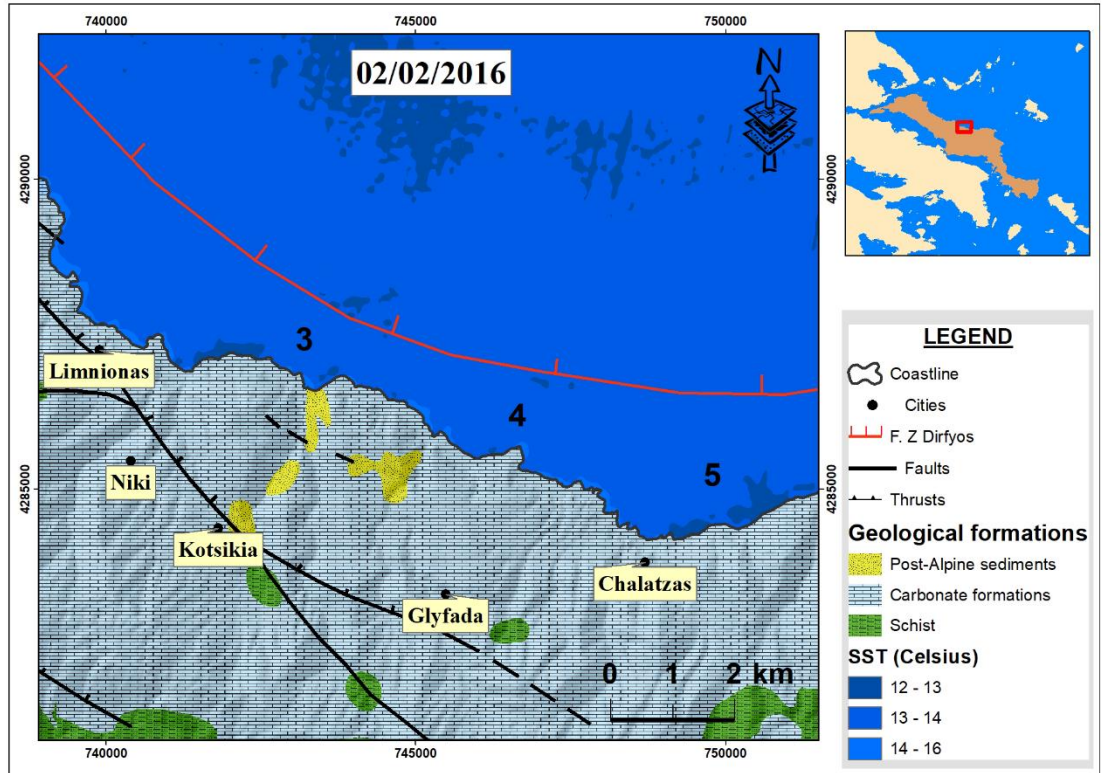


**Fig. 4:** Freshwater outflows areas of Evia.

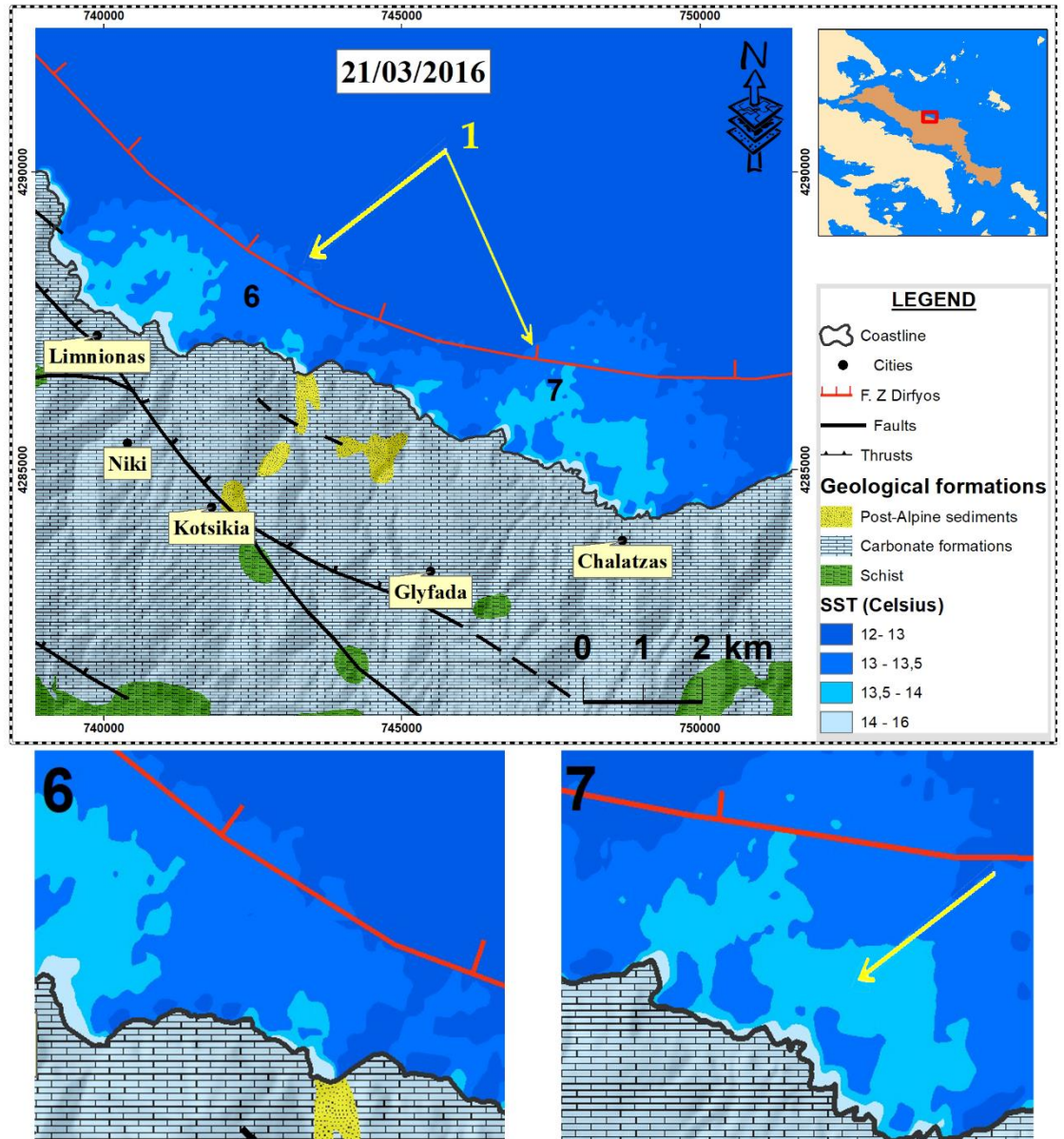
1. January



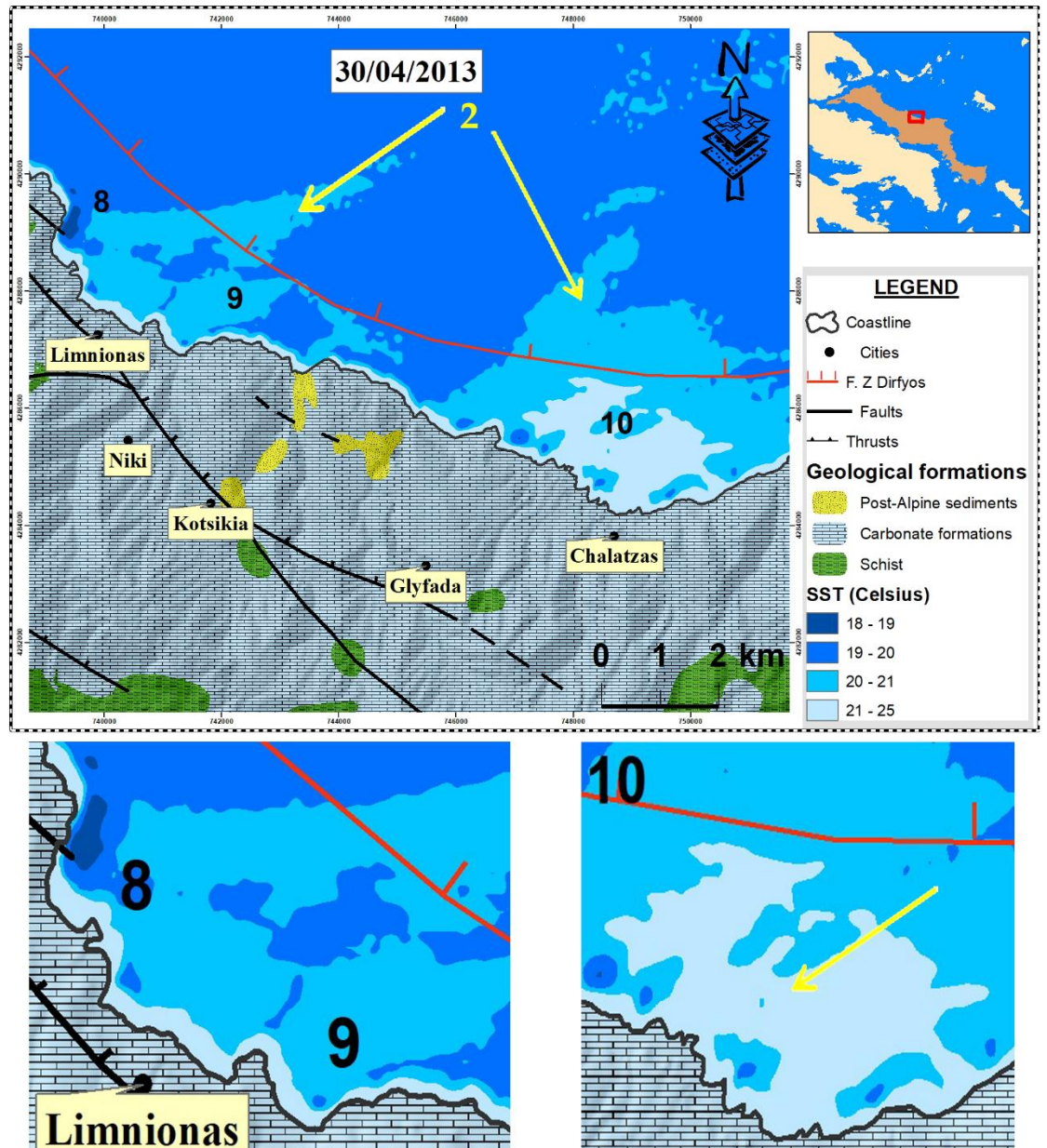
2. February



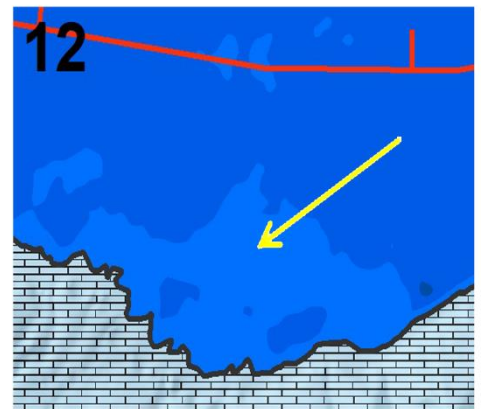
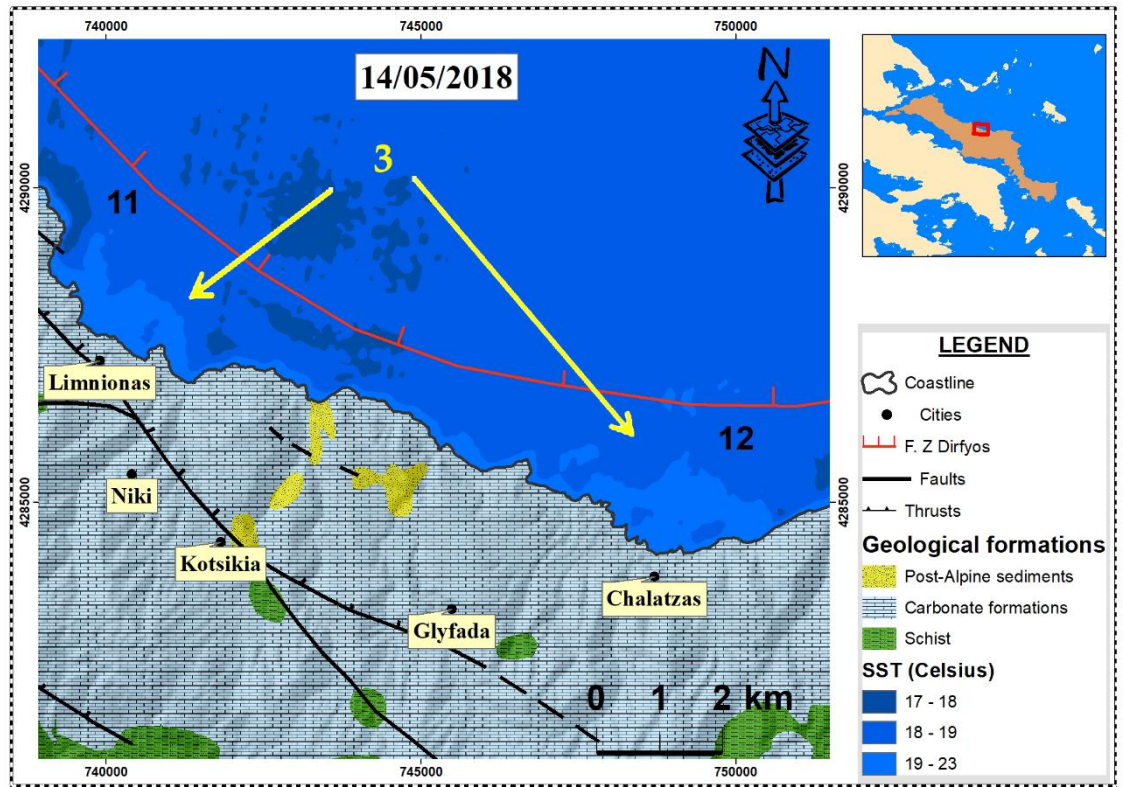
3. March



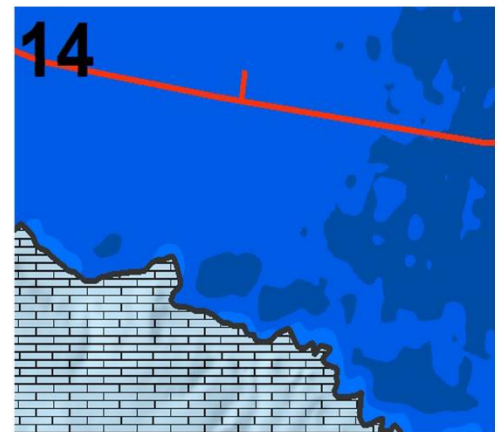
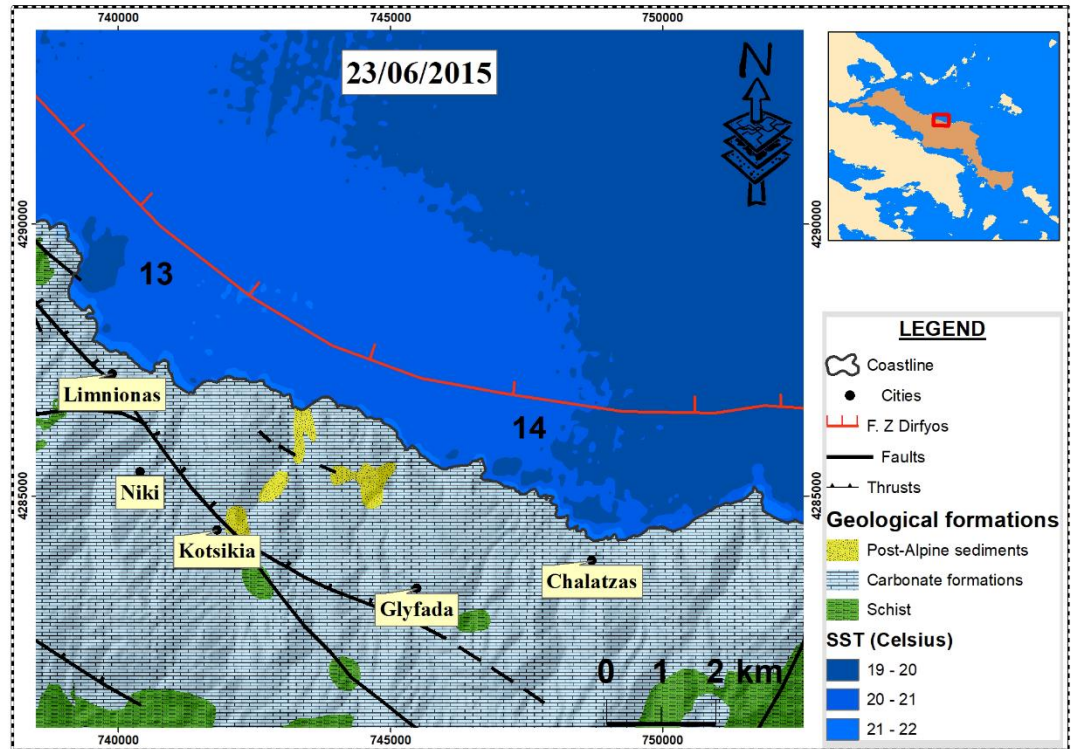
4. April



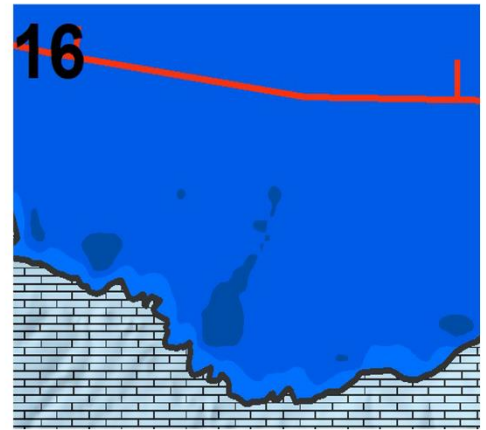
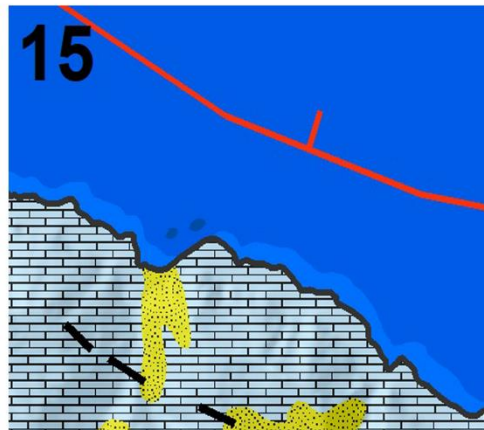
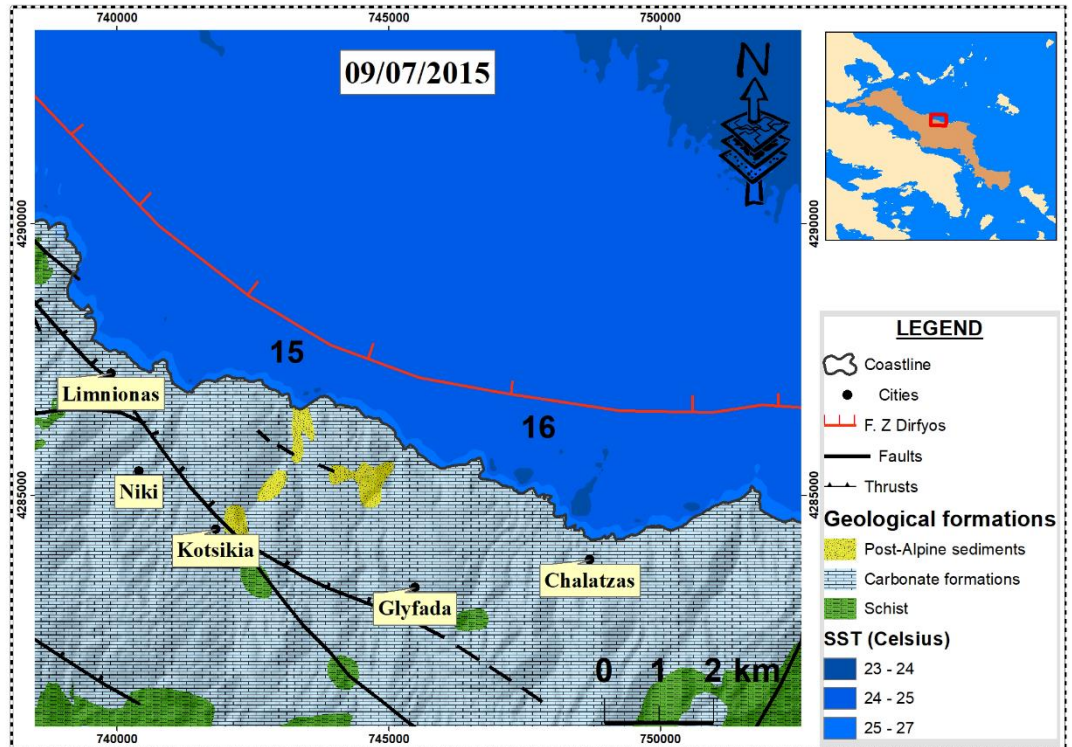
5. May



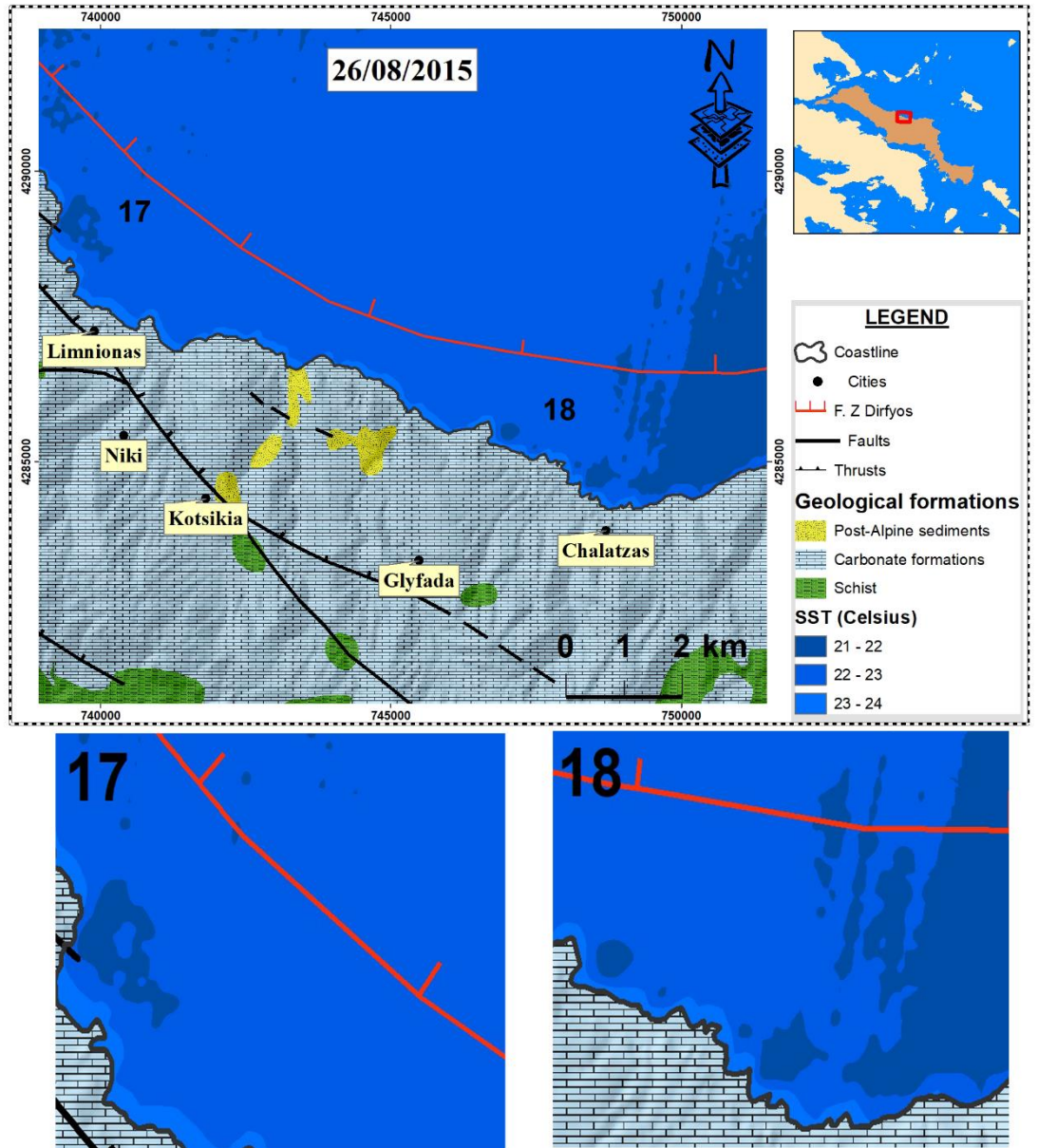
6. June



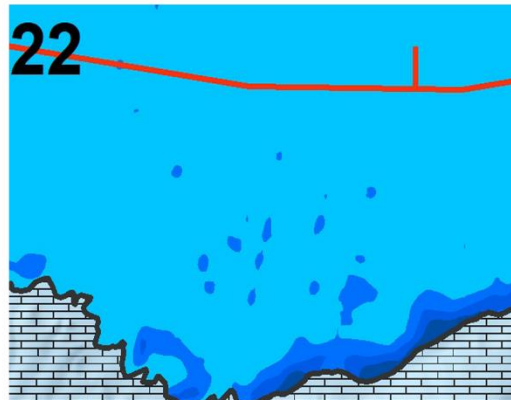
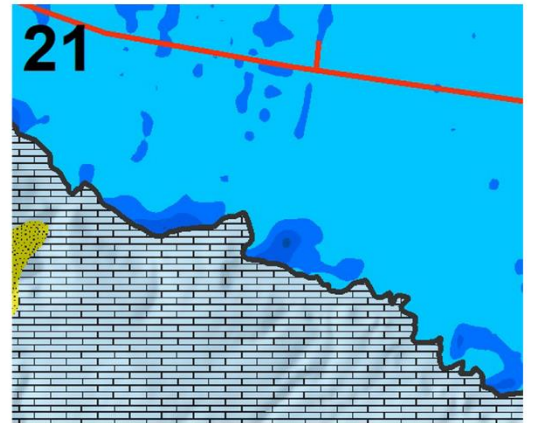
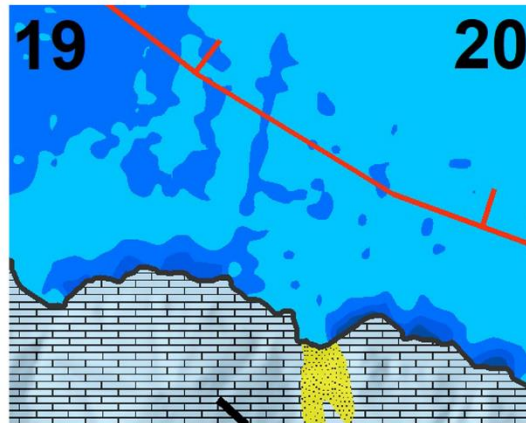
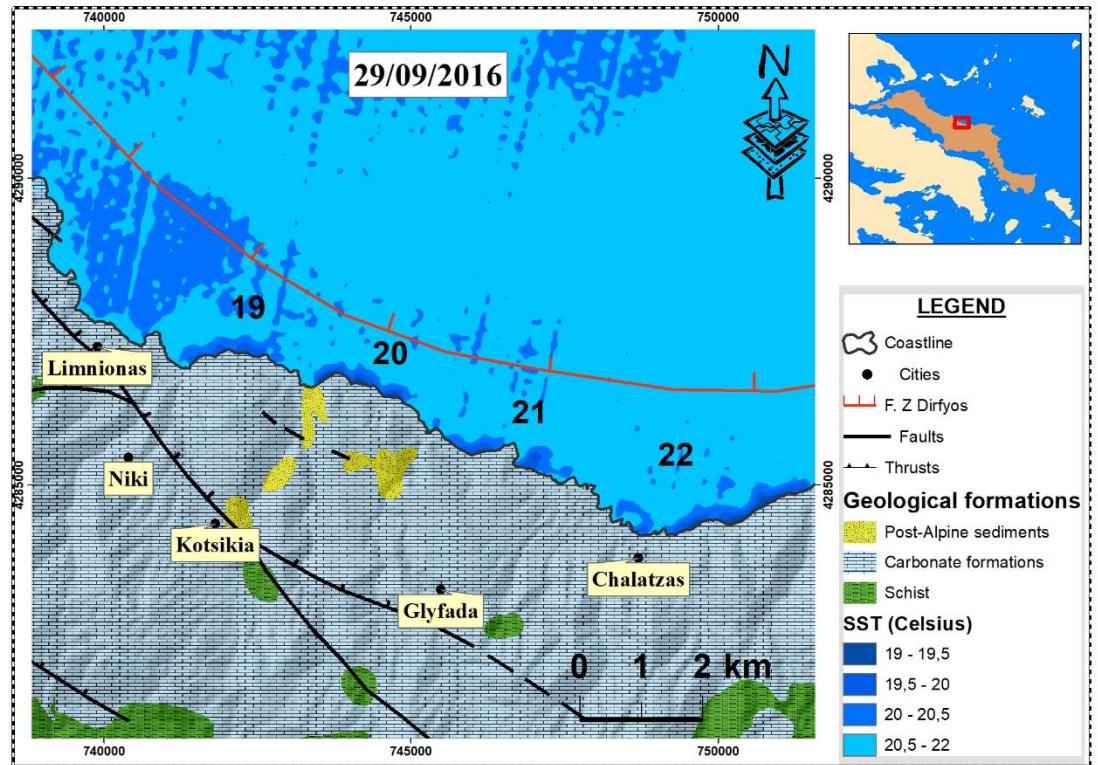
7. July



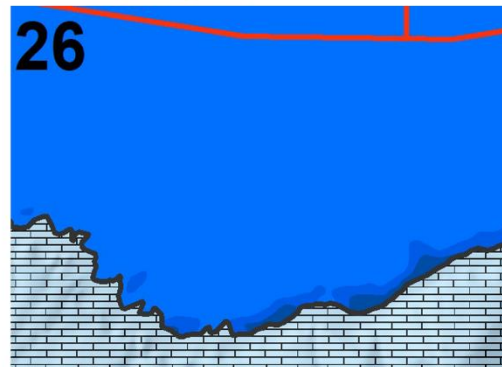
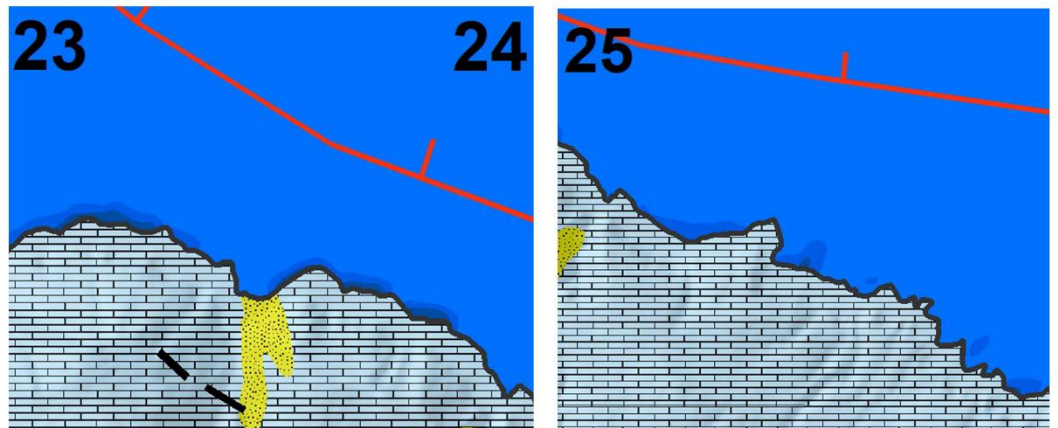
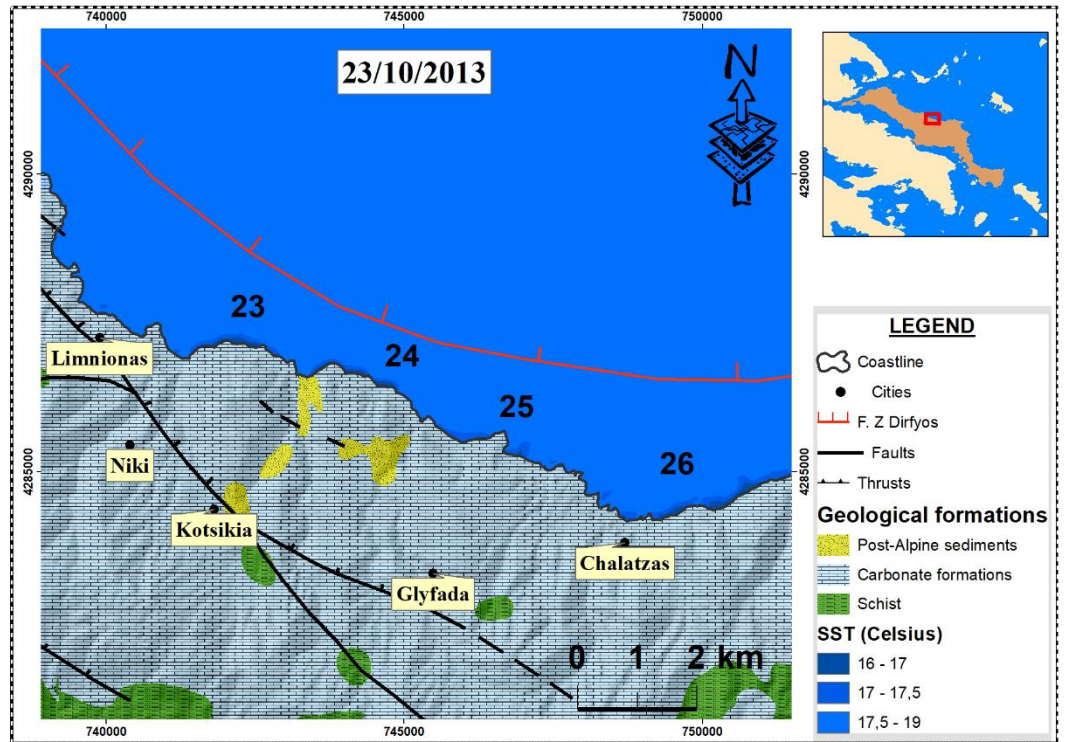
8. August



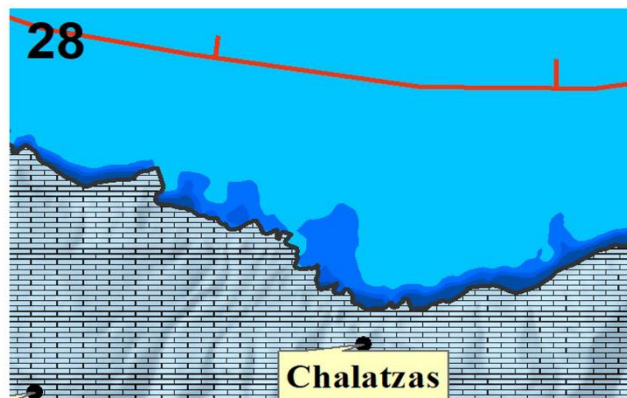
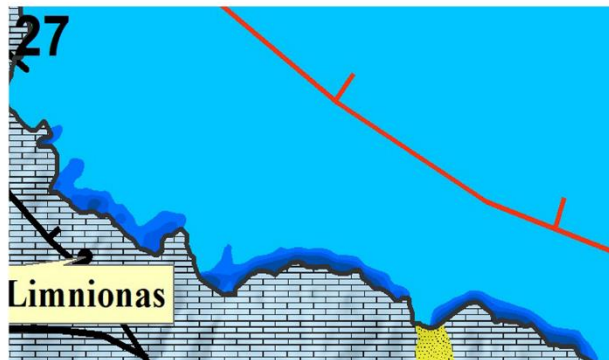
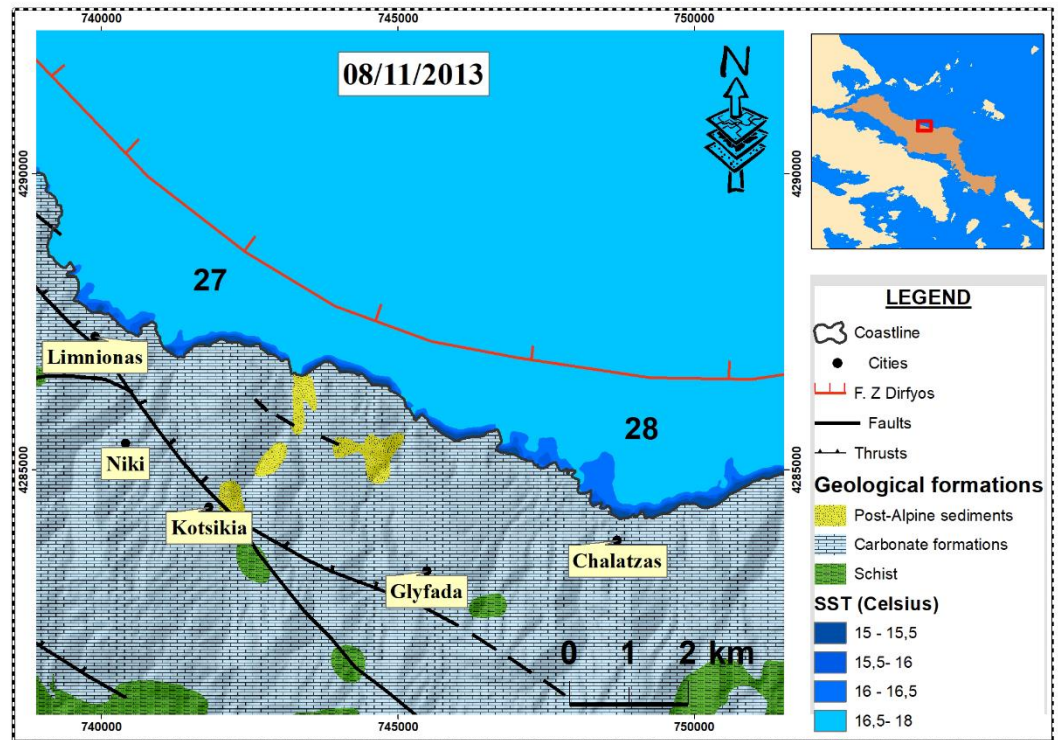
9. September



10. October



11. November



12. December

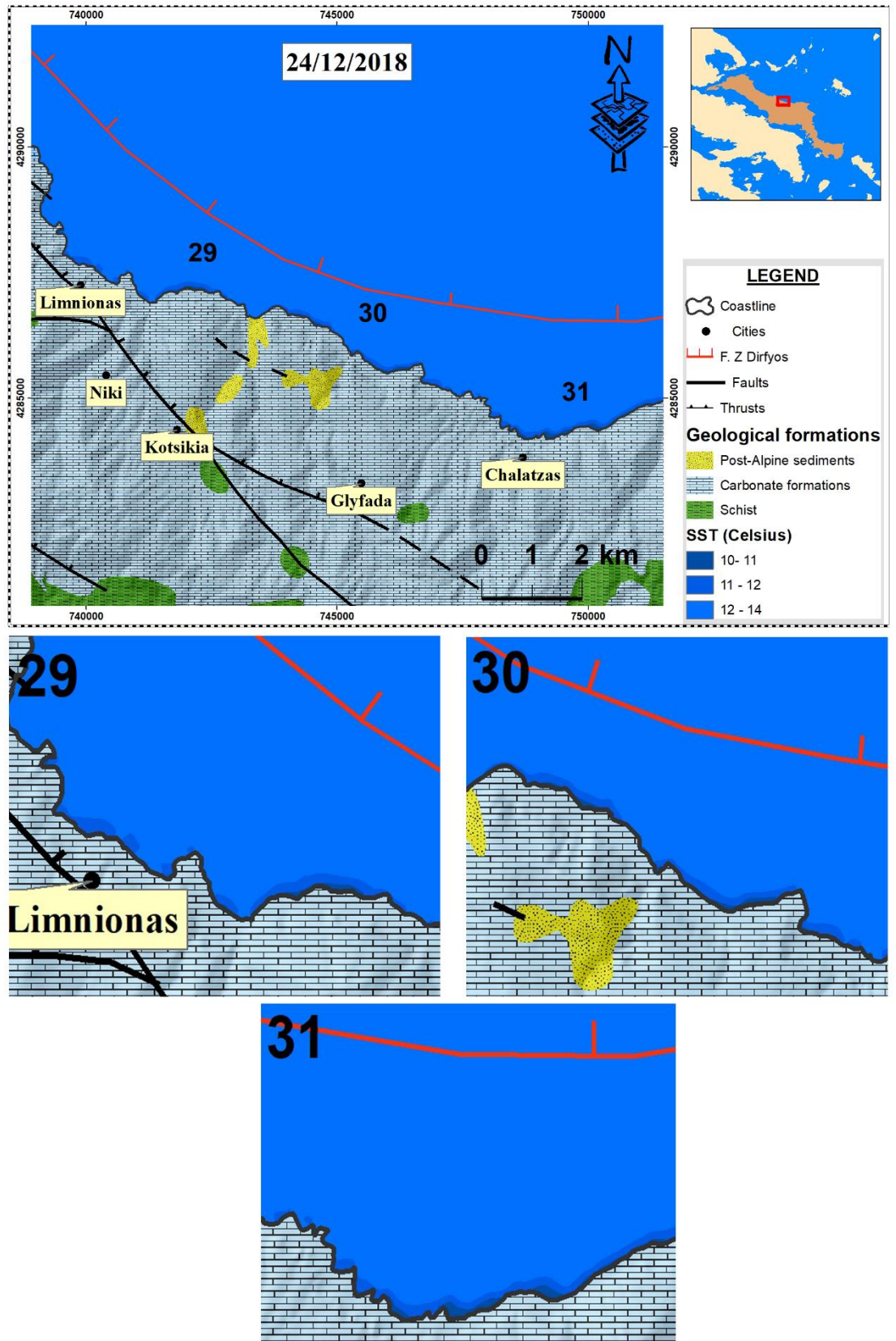


**Fig. 5:** SST maps and freshwater outflows illustrated on twelve images from 2013 to 2018.

## 5. CONCLUSIONS

Part of Evia Island's coastline is formed by carbonate formations. The present coastal karst base level is a consequence of Alpine Orogeny's tectonic movements with the vertical eustatic movements in the Quaternary period. Coastal aquifers tend to discharge their subsurface flow into the sea through coastal or submarine springs, which appear in tectonic discontinuities. Remote Sensing gives the capability to identify freshwater outflows based on thermal anomalies in the sea surface. In this study, spectral band 10 of Landsat 8 TIRS (high gain) images between 2013 and 2018 were used to estimate the temperature of the freshwater plumes. G.I.S was used to combine geologic, topographic maps and thermal images to create sea surface temperature maps (SST). The results show that the integrated, synergistic use of Remote Sensing and GIS has been proved useful in analysing the phenomenon of cold groundwater discharge towards the sea. Based on the analysis, a number of spots, where freshwater flows into the sea along the coastal zone, were detected and are controlled by the presence of faults that act as zones that increased the permeability and hydraulic conductivity in the carbonate terrain of the outflows areas. In conclusion, Remote Sensing and G.I.S are noteworthy and powerful tools for groundwater outflow monitoring and management of submarine groundwater discharge in coastal waters and providing information to supplement the conventional field data.

## 6. REFERENCES

- Alshaikh, A. Y., 2016. Detection of Sea Surface Temperature and Thermal Pollution of Agricultural Coastal Areas using Thermal Infrared, Jeddah City, West KSA. *Global Advanced Research Journal of Agricultural Science*, 5(1), 051-060.
- Astaras, T., 2001. The present state remote sensing applications to multitemporal monitoring of the environment, with emphasis to delineation of coastal plain areas suffering from salt water encroachment (intrusion) and to detection of water discharge in coastal rocky (mainly karstic) environment. Future prospects. *A keynote lecture presented at the 9th MCM of COST 621 Meeting in Venice, Italy, March 22-24.*
- Buettner, K. J. K., Kern C. D., 1965. The determination of infrared emissivities of terrestrial surfaces. *J. Geophys. Res.*, 70, 1329–1337.
- Cavinato, G.P., De Celles, P.G., 1999. Extensional basins in the tectonically bimodal Central Apennines fold-thrust belt, Italy: response to corner flow above a subducting slab in retrograde motion. *Geology* 27, 955–958.

- Chander, G., Markham, B.L., Helder, D.L., 2009. Summary of current radiometric calibration coefficients for Landsat MSS, TM, ETM+, and EO-1 ALI sensors. *Remote Sensing of Environment*, 113, 893–903.
- Chavez, P.T., 1988. An improved dark-object subtraction technique for atmospheric scattering correction of multispectral data. *Remote Sensing of Environment*, 24 (3), 459–479.
- Das, S., Vettiyattil, M. R., Thilakan S.P., 2010. Validation of Potential Fishing Zones along Saurashtra Coast, Gujarat. *Coastal Fishery Resources of India - Conservation and Sustainable Utilisation*, 1, 138- 144.
- Davies, J. A., Robinson P. J., and Nunez M., 1971. Field determination of surface emissivity and temperature for Lake Ontario. *J. Appl. Meteor.*, 10, 811–819.
- Donlon, C.J.; Minnett, P.J.; Gentemann, C.; Nightingale, T.J.; Barton, I.J.; Ward, B.; Murray, M.J., 2002. Toward Improved Validation of Satellite Sea Surface Skin Temperature Measurements for Climate Research. *J. Clim.*, 15, 353–369.
- Fingas, M., Brown, C.J., 2018. A Review of Oil Spill Remote Sensing. *Sensors (Basel)*, 1, 91.
- Fleury, P., Bakalowicz, M., de Marsily, G., 2007. Submarine springs and coastal karst aquifers: A review. *Journal of Hydrology*, 339, 79-92.
- Fotiadis A., forthcoming publication. Geologic map of Greece, scale 1:50,000, Steni Dirfyos sheet, Institute of Geology and Mineral Exploration (IGME).
- Ganas, A., and Stefouli M., 1995. Sea surface temperature measurements in Central Aegean utilizing Landsat TM data. Proceedings of the 4th International Conference of the Hellenic Geographical Society, Athens, p. 417-429 (In Greek).
- Ganas, A., Vassilopoulou, S., Sakkas, V., Lagios, E., Dietrich, V., Hurni, L., and Stavrakakis, G., 2003. Thermal Monitoring of Nissyros Volcano (Greece) by Digital Processing of Satellite Data. Contribution EAE03-A-09945 for the EGS - AGU - EUG Joint Assembly, Nice, France.
- Ganas, A., and Lagios, E., 2003. Landsat 7 Night Imaging of the Nissyros volcano, Greece. *International Journal of Remote Sensing*, 24 (7), 1579–1586.
- Ganas, A., Pavlides, S., Karastathis, V., 2005. DEM-based morphometry of range-front escarpments in Attica, central Greece, and its relation to fault slip rates. *Geomorphology*, 65, 301–319.

Gibbons, D.E., Wukelic, G.E., Leighton, J.P., Doyle, M.J., 1989. Application of Landsat Thematic Mapper data for coastal thermal plume analysis at Diablo Canyon. *Photogrammetric Engineering and Remote Sensing* 55, 903-909.

Gittings, J.A., Raitzos, E.D., Krokos, G., Hotei, I., 2018. Impacts of warming on phytoplankton abundance and phenology in a typical tropical marine ecosystem. *Scientific Reports*, 8, Article number: 2240.

Goldsworthy, M., Jackson, J. & Haines, J., 2002. The continuity of active fault systems in Greece. *Geophysical Journal International*, 148(3), 596-618.

Häuselmann P, Yves Jeannin P, Bitterli T, 1999. Relationships between karst and tectonics: case-study of the cave system north of Lake Thun (Bern, Switzerland). *Geodynamica Acta*, 12(6), 377–387.

Hellenic Army Geographic Service (HAGS), 18 Map Sheets, 1:50.000 Scale.

Hemalatha, M., & Varadarazan, S., 2018. Feature Enhancement of Multispectral images using vegetation, water, soil indices image fusion. *Proceedings of the International Conference on ISMAC in computational vision and Bio-Engineering*, 329–338.

<https://earthexplorer.usgs.gov>

[https://www.usgs.gov/special-topic/water-science-school/science/desalination?qt-science\\_center\\_objects=0#qt-science\\_center\\_objects](https://www.usgs.gov/special-topic/water-science-school/science/desalination?qt-science_center_objects=0#qt-science_center_objects)

<https://landsat.gsfc.nasa.gov/landsat-8/>

<https://en.wikipedia.org/wiki/Euboea>

Jiménez-Muñoz J, Sobrino J. A, Gillespie A., Sabol D., Gustafson W. T., 2006. Improved land surface emissivities over agricultural areas using ASTER NDVI. *Remote Sens. Environ.*, 103(4), 474–487.

Kallioras, A., Pliakas, F., Marinos, P., 2016. Groundwater resources assessment of granular aquifers in Greece. *Proceedings of the 14<sup>th</sup> International Congress*, Thessaloniki, p.701-709.

Kang, Ki-mook, et al. 2014. Comparison of Coastal Sea Surface Temperature derived from Ship-, Air-, and Space-borne Thermal Infrared Systems. *International Geoscience and Remote Sensing Symposium*, pp. 4419-4422.

- Karfakis, I., Stefouli, M., Tsombos, P., 1998. Identification and monitoring of water outflows in coastal areas using remote sensing techniques. Case studies in Greece". Eurisys Colloquium, Athens.
- Karfakis, I., Nikolakopoulos, K., 2003. Landsat TM images for the detection of water outflows in the coastal area of South Attiki Peninsula, Greece. *Proceedings of SPIE*, 4881, p. 692-700.
- Katsikatsos, G., Mercier, Vergely, J. P., 1976b. La fenetre d Attique. Cyclades et des fenetres metamorphiques des Hellenides internes (Grece). C.R Acad. Sc. Paris, 283, D., 1614 -1616, Paris.
- Katsikatsos, G., 1992. Geology of Greece, Study and Teaching, University of Patras.
- Katsikatsos, G. Koukis, G., Mettos., A., 1978. Geologic map of Greece, scale 1:50,000, Larymna sheet, Institute of Geology and Mineral Exploration (IGME)
- Katsikatsos, G., Mettos, A., Vidakis, M., Kounis, G., Fytikas, M., 1980. Geologic map of Greece, scale 1:50,000, Limni sheet, Institute of Geology and Mineral Exploration (IGME)
- Katsikatsos, G., Fytikas, M., Koukis, G., Anastopoulos, I., Tsaila-Monopolis, St., 1981. Geologic map of Greece, scale 1:50,000, Kymi sheet, Institute of Geology and Mineral Exploration (IGME).
- Katsikatsos, G., Koukis, G., Fytikas, M., Anastopoulos, I., Kanaris, J., Tsaila-Monopolis, St., 1981. Geologic map of Greece, scale 1:50,000, Psaxna - Pilion sheet, Institute of Geology and Mineral Exploration (IGME).
- Katsikatsos, G., Mettos, A. and Vidakis, M., 1984. Geologic map of Greece, scale 1:50,000, Istiaia sheet, Institute of Geology and Mineral Exploration (IGME).
- Katsikatsos, G., Premoli-Silva, I., Kollmann, H., Zapfe, H., Sauvage, I., de Bruijn, H., der Meulen, V., Brother, 1977. Geologic map of Greece, scale 1:50,000, Aliveri sheet, Institute of Geology and Mineral Exploration (IGME).
- Katsikatsos G., 1991. Geologic map of Greece, scale 1:50,000, Rafina sheet, Institute of Geology and Mineral Exploration (IGME)
- Katsikatsos G., 2000. Geologic map of Greece, scale 1:50,000, Eretria sheet, Institute of Geology and Mineral Exploration (IGME).
- Katsikatsos G. and Koukis G., 2007. Geologic map of Greece, scale 1:50,000, Chalkida sheet, Institute of Geology and Mineral Exploration (IGME).

- Kay S, John D., Lavender H & S., 2005. Sun Glint Correction of High and Low Spatial Resolution Images of Aquatic Scenes: a Review of Methods for Visible and Near-Infrared Wavelengths. *Remote Sens.* 2009, 1, 697-730.
- Kelepertsis A, Tziritis E., Kelepertzis E., Leontakianakos G., Palla K., 2009. Hydrogeochemical characteristics and genetic implications of Edipsos thermal springs, north Euboea, Greece. *Open geosciences*, 1, 241-25.
- Konda M., Katsuya N. I, Toda N.T., 1994. Measurement of the sea surface emissivity. *Journal of Oceanography*, 50 (1), 17–30.
- Korozis, S., 2011. Geological and seismotectonic conditions in the Chalkida area and their impact on the construction works. Graduate thesis. School of Mining and metallurgical Engineering, National Technical University of Athens (In Greek).
- Kuz'mina, E.A., Novopashina, A.D., 2018. Groundwater outflows and fault density spatial relation in the Baikal rift system (Russia). *Italian Journal of Groundwater*, 317: 19-27.
- Lamaro, A.A., Marinelarena, A., Torrusio, S.E., Sala, S.E., 2013. Water surface temperature estimation from Landsat 7 ETM+ thermal infrared data using the generalized single-channel method: Case study of Embalse del Río Tercero (Córdoba, Argentina). *Advances in Space Research*, 51, 492-500.
- Latsouda X., and Triantafilli M., 1997. Geologic map of Greece, scale 1:50,000, Karistos sheet, Institute of Geology and Mineral Exploration (IGME).
- Lekkas, E., 2002. Operational Organization of Chalkida Town Planning Group for Seismic Risk Management. Department of Dynamics, Tectonics and Applied Geology, National and Kapodistrian University of Athens (In Greek).
- Lancia, M., Zheng, C., Yi S., Lerner D.N., Andrews C., 2018. Analysis of groundwater resources in densely populated urban watersheds with a complex tectonic setting: Shenzhen, southern China. *Hydrogeology Journal*, 27(1):183-194.
- Mallast, U., Siebert, C., Wagner, B., Sauter, M., Gloaguen, R., Geyer, S., Merz, R., 2013. Localisation and temporal variability of groundwater discharge into the Dead Sea using thermal satellite data. *Environmental Earth Sciences*, 69(2): 587-603.
- Masud, J.M, and Bastiaanssen Wim, G. M., 2017. Remote Sensing and GIS Applications in Water Resources Management. Chapter 16, in: Allah Bakhsh and Muhammad Rafiq (Eds), Choudhry University of Agriculture, Faisalabad, Pakistan, 351-373 pp..

- Masuda, K., T. Takashima and Takayama Y., 1988. Emissivity of pure and sea waters for the model sea surface in the infrared window regions. *Remote Sens. Environ.*, 24, 313–329.
- McFeeters, S. K., 1996. The use of the normalized difference water index (NDWI) in the delineation of open water features. *International Journal of Remote Sensing*, 17(7), 1425–1432.
- Meijerink, A.M.J., Bannert, D., Batelaan, O., Lubczynski, M.W., Pointet, T., 2007. Remote Sensing applications to groundwater. IHP-VI Series on Groundwater, No16, Published by the United Nations Educational-Scientific and Cultural Organization, pp. 89-94.
- Mikhaylov, B. A. and V. M. Zolotarev (1970): Emissivity of liquid water. *Atmos. Oceanic Phys.*, 6, 52.
- Migiros, G., Psomiadis, E., Papanikolaou, I., Karamousalis, T., Stamatis, G., 2008. Groundwater coastal discharge of the karstic system of the Mani Peninsula, Southern Peloponnesus-Greece. *Proceedings of the 8<sup>th</sup> International Congress of Hydrogeology*, 1, p. 317-326.
- Ompetsanof, I., Koumantakis, I., Stamataki, S., 2004. Karstic springs in Greece. Survey and Evaluation Using Geographical Information System (GIS). *Technical Annals*, March-April, 2, p.22 (In Greek).
- Palyvos, N., Bantekas, I., Kranis, H., 2006. Transverse fault zones of subtle geomorphic signature in northern Evia island (central Greece extensional province): An introduction to the Quaternary Nileas graben. *Geomorphology*, 76(3-4): 363-374.
- Papanikolaou, D., 2009. Timing of tectonic emplacement of the ophiolites and terrane paleogeography in the Hellenides, *Lithos*, 108, 262–280.
- Parcharidis, I., Psomiadis, E., Stamatis, G., 1998. Using Landsat TM images to study karstic phenomenon. *ITC Journal*, 2, 118-123, Netherland.
- Petitta M., 2009. Hydrogeology of the middle valley of the Velino River and of the S. Vittorino Plain (Rieti, Central Italy). *Ital J Eng Geol Environ* 1:157–181.
- Roberts, S., Jackson, J.A., 1991. Active normal faulting in Central Greece: an overview. In: Roberts, A.M., Yielding, G. & Freeman, B. (eds) *The Geometry of Normal Faults*. *Geological Society, London, Special Publications*, 56, 125–142.

- Saunders, P. M., 1967b. Aerial measurement of the sea surface temperature in the infrared. *J. Geophys. Res.*, 72, 4109–4117.
- Saunders, P. M., 1968. Radiance at sea and sky in the infrared window 800–1200 cm<sup>-1</sup>. *J. Opt. Soc. Amer.*, 58, 645– 652.
- Snyder W. Wan, Y C, Z. Zhang & Feng, Y.-Z., 1988. Classification-based emissivity for land surface temperature measurement from space. *International Journal of Remote Sensing.*, 19 (14), 2753-2774.
- Stefanakis, A., Charalampopoulos, I., Psomiadis E., Prigent S., 2018. The thermal regime of a large Constructed Wetland in the desert environment. *Proceedings of IWA Specialist Conference on Wetland Systems of Water Pollution Control*, Valencia, Spain, p.1-4.
- Stefouli, M., Tsombos P., 2004. Identification and monitoring of freshwater outflows in coastal areas: pilot study on Psahna area/Evia Island-Greece. *Proceedings of the 10<sup>th</sup> International Congress*, Thessaloniki, p. 928-937.
- Tang, D.; Kester, D.R.; Wang, Z.; Lian, J.; Kawamura, 2003. H. AVHRR satellite remote sensing and shipboard measurements of the thermal plume from the Daya Bay, nuclear power station, China. *Remote Sens. Environ*, 84, 506–515.
- Tcherepanov, E.N., Zlotnik V.A., Henebty G.M., 2005. Using Landsat thermal imagery and GIS for identification of groundwater discharge into shallow groundwater-dominated lakes. *International Journal of Remote Sensing*, 26 (17), 3649-3661.
- Theilen-Willige, B., Malek, H.A., Charif, A., El Bchari, F., Chaibi, M., 2014. Remote Sensing and GIS contribution to the investigation of Karst landscaped in NW-Morocco. *Geosciences*, 4, 50-72.
- UNESCO, 1978. World water balance and water resources of the earth. Publ: Paris.
- USGS - U.S. Geological Survey, Department of the Interior, 2016. Landsat 8 (L8) data users hand book, Version 2.0, EROS Sioux Falls, South Dakota.
- Valkanou, K., Karimpalis, K., Papanastasiou D., Soldati, M., Chalkias Ch., Gaki-Papanastasiou, K., 2015. The impact of tectonics on river systems in northern Euboea, Central Greece. Theofrastos Digital Library - Department of Geology. AUTH Thessaloniki (In Greek).